Engineering xxx (xxxx) xxx

Contents lists available at ScienceDirect

Engineering

journal homepage: www.elsevier.com/locate/eng

Research
Low Carbon Transformation for Conventional Energies—Article

Towards Carbon-Neutral Ironmaking: Stepwise Integration of Biocarbon in PCI with Combustion Behavior Characterization and Injection Limit Evaluation

Min-Woo Kim [a], Min-Jong Ku [a], Jongho Kim [b], Gyoung-Min Kim [c], Chung-Hwan Jeon [a,c,*], Dae-Gyun Lee [d,**]

[a] School of Mechanical Engineering, Pusan National University, Busan 46241, the Republic of Korea
[b] Ironmaking Research Group, POSCO Technical Research Laboratories, Pohang 790785, the Republic of Korea
[c] Pusan Clean Energy Research Institute, Pusan National University, Busan 46241, the Republic of Korea
[d] Mechanical Engineering, Dong-Eui University, Busan 47340, the Republic of Korea

ARTICLE INFO

Article history:
Received 2 September 2025
Revised 9 November 2025
Accepted 10 December 2025

Keywords:
Blast furnace
Biomass
Maximum injection limit
Torrefaction
Biochar

ABSTRACT

As the steel industry is intended to be carbon-neutral, transitional solutions are required before full-scale hydrogen-based reduction becomes viable. One such strategy is the partial replacement of pulverized coal injection (PCI) with high-quality biocarbon in blast furnace (BF) operations. Raw biomass presents challenges, such as low grindability, high ash content, and low energy density, which can be mitigated through torrefaction and carbonization. This study evaluates the combustion behavior and injection limits of four biocarbon samples (mildly torrefied biomass (MTB), hard torrefied biomass (HTB), mildly carbonized biomass (MCB), and hard carbonized biomass (HCB)) using thermogravimetric analysis (TGA), drop tube furnace (DTF), and laminar flow reactor (LFR) experiments. Results show that as biomass is carbonized, its combustion kinetics increasingly resemble those of PCI coal. Co-firing tests confirmed improved performance at higher blending ratios, especially with highly treated samples, such as HCB, due to enhanced fragmentation and char reactivity. Injection limits were determined based on combustion performance, heating value (±5% of PCI coal), and ash content (< 10%). The MTB and HCB exceeded these limits at approximately 27%–30% blending, indicating the need for an adjusted fuel input. Overall, biocarbon shows strong potential as a PCI substitute, offering a feasible low-carbon pathway for existing BF systems.

1. Introduction

The blast furnace (BF) process has long been recognized as the principal source of CO_2 emissions in the iron and steel industry. International Energy Agency reported that the global steel sector has emitted approximately 2.8 Gt of CO_2 annually, accounting for approximately 8% of the total anthropogenic greenhouse gas emissions worldwide [1,2]. CO_2 is primarily generated during the reduction of iron ore using coke and pulverized coal (PC) as well as from the combustion of BF off-gases [3]. In particular, the BF-basic oxygen furnace (BF-BOF) integrated steelmaking route emits approximately 1.8–2.0 tonnes of CO_2 per tonne of hot metal produced [4]. Given this considerable emission intensity, the BF process has become a major target for decarbonization strategies in the ironmaking sector.

To reduce CO_2 emissions from BF operations, alternative ironmaking technologies, such as shaft-based direct reduction and the FINEX process, developed by POSCO in Korea, have been adopted as transitional solutions toward hydrogen-based steelmaking [2,5–7]. These technologies aim to gradually increase the use of hydrogen as a reductant of CO_2 emission by fossil fuels. The FINEX process utilizes a combination of carbon monoxide (CO) and H_2 gases derived from a melter-gasifier to reduce iron ore in a fluidized bed, with hydrogen accounting for approximately 25% of the reducing gas mixture [2,6,7]. However, the shift toward

* Corresponding author at: School of Mechanical Engineering, Pusan National University, Busan 46241, the Republic of Korea.
** Corresponding author at: Mechanical Engineering, Dong-Eui University, Busan 47340, the Republic of Korea.
E-mail addresses: chjeon@pusan.ac.kr (C.-H. Jeon), gangoo8@naver.com (D.-G. Lee)..

https://doi.org/10.1016/j.eng.2025.12.004

fully hydrogen-based ironmaking remains challenging. The high production cost of green hydrogen, currently estimated at 3–8 USD·kg^{-1}, combined with the substantial energy demands for storage, liquefaction, and transport, poses significant limitations to its economic feasibility [8,9]. Furthermore, the system optimization and scaling of hydrogen-based reduction reactors, such as HyREX or shaft furnaces, remain in the early developmental stages [3,4,10]. Because of these technological and infrastructural limitations, a direct transition to carbon-free hydrogen reduction is currently impractical. Therefore, a stepwise approach involving the partial replacement of PC with carbon-neutral biogenic fuels such as biocarbon is considered a viable interim strategy [3,7].

In recent years, biomass-based fuels, particularly torrefied biomass and biochar, have gained global attention as transitional alternatives for PC injection (PCI) in BF operations. In Japan, Kobelco (Kobe Steel) announced plans to apply torrefied wood pellets developed by MUCC to the Kakogawa Works BF as part of an initial pilot-scale test [11]. In India, the state-owned SAIL company conducted PCI co-firing trials using biochar and charcoal at BF-1 of the Rourkela Steel Plant in August 2024, evaluating indigenous biomass sources, such as bamboo and babul wood [12]. In Canada, ONYM Energy is constructing a commercial-scale biochar plant in partnership with ArcelorMittal to supply up to 15 000 tons per year for use in BF operations, with an expected CO_2 reduction of approximately 70 000 tons annually [13]. In the United States, the Natural Resources Research Institute of Minnesota has actively developed biochar briquettes for electric arc furnace (EAF) applications [14]. These efforts, ranging from Japan's torrefied pellet initiatives and India's PCI co-firing demonstrations to Canada's industrial biochar production and the United States EAF-focused developments, underscore the growing interest in biomass as a viable carbon-neutral fuel in the steel sector.

However, all these studies emphasize the importance of pretreatment techniques such as torrefaction or pyrolysis to ensure desirable fuel characteristics, including heating value, particle size, moisture content, and flowability [15–17].

As shown in Fig. 1, in European countries, approximately 300–400 kg of coke is consumed per ton of hot metal produced in BFs, along with the injection of various supplemental fuels [17]. In addition to conventional PC, a significant portion of PC fuel is being replaced by alternative fuels, such as bio-oil, wood pellets, hardwood-derived charcoal, and torrefied biomass. When calculating the replacement ratios, wood pellets can substitute PC fuel at a ratio of approximately 1:1.91, torrefied biomass ranges from 1:1.4 to 1:1.7, and hardwood charcoal can replace PC at almost a 1:1 ratio. As biomass fuels undergo thermal treatment, their properties become increasingly similar to those of PC fuels, enabling effective substitution. Furthermore, stable combustion can be achieved within a raceway in which PC combustion typically occurs.

Recent studies have approached biomass utilization from both system-level carbon mitigation and process-level reaction mechanisms. At the policy and resource management scale, municipal solid waste classification has been evaluated in terms of its influence on carbon emissions and regional carbon-neutrality strategies [18]. At the combustion system level, co-combustion of biomass with anthracite in circulating fluidized bed (CFB) boilers has been shown to affect ash thermomechanical behavior and operational stability [19]. Under chemical looping environments, agricultural biomass ash and phosphate-containing species have been demonstrated to alter the surface structure and redox performance of ilmenite oxygen carriers, indicating degradation pathways and the need for regeneration or replacement strategies [20,21]. In parallel, combustion chemistry studies have compared NO and N_2O formation mechanisms across NH_3/H_2 combustion regimes, providing insights relevant to integrating zero-carbon fuels into biomass-based systems [22]. Beyond combustion, molten salt–mediated biomass gasification with *in situ* CO_2 capture has been proposed as a route to high-yield hydrogen production, positioning biomass as a feedstock for low-carbon hydrogen systems rather than solely as a supplemental solid fuel [23]. Collectively, these works illustrate a continuum from waste-resource carbon accounting to fuel reactivity, material compatibility, and hydrogen-oriented biomass conversion.

To utilize biomass as a viable PCI fuel, pretreatment is essential due to its inherently low heating value, high ash content, and poor grindability. As shown in Fig. 2, among the various carbonization methods, torrefaction and biochar production (via pyrolysis or ashless treatment) can improve biomass characteristics to levels comparable to those of coal. Torrefaction, performed at 473–573 K in an oxygen-deficient atmosphere, reduces moisture and volatiles, enhances fixed carbon content, and improves grindability. According to Lee et al. [24], torrefied pine and kenaf show increased fuel-N content, resulting in higher NO_x emissions, particularly from herbaceous biomass.

Although torrefaction improves energy density and hydrophobicity, its effect on emissions should be carefully evaluated. Alternatively, ashless treatment, as demonstrated in a follow-up study [25], can significantly remove alkali and alkaline earth metals

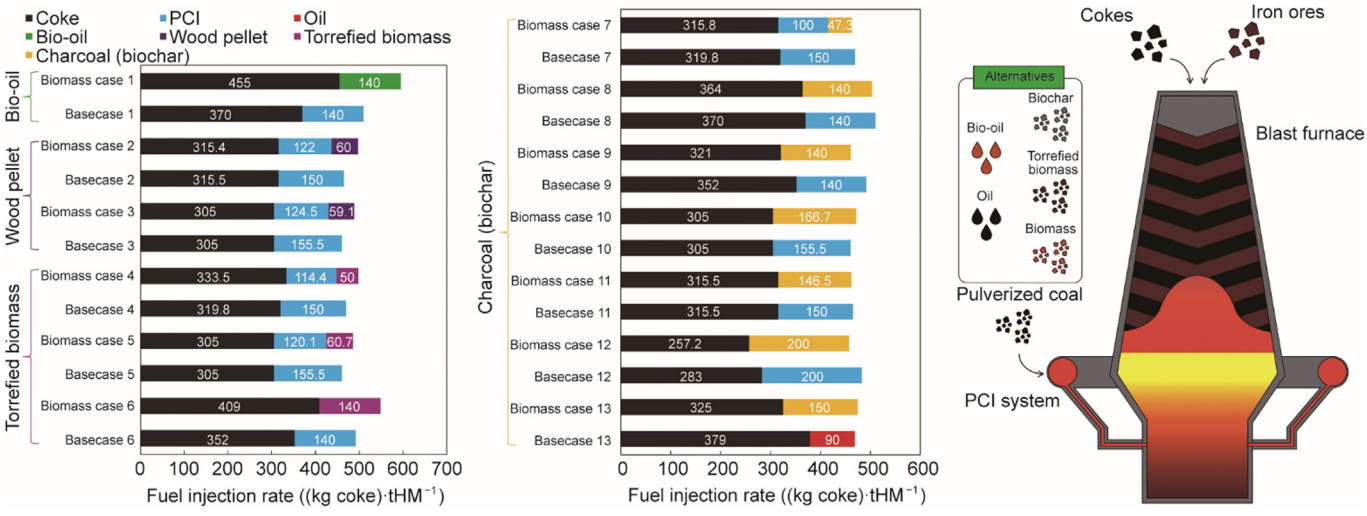

Fig. 1. Fuel injection rate of alternative fuel (biomass, torrefied wood pellet, biocarbon, and so forth) cases in BF. tHM: ton of hot metal.

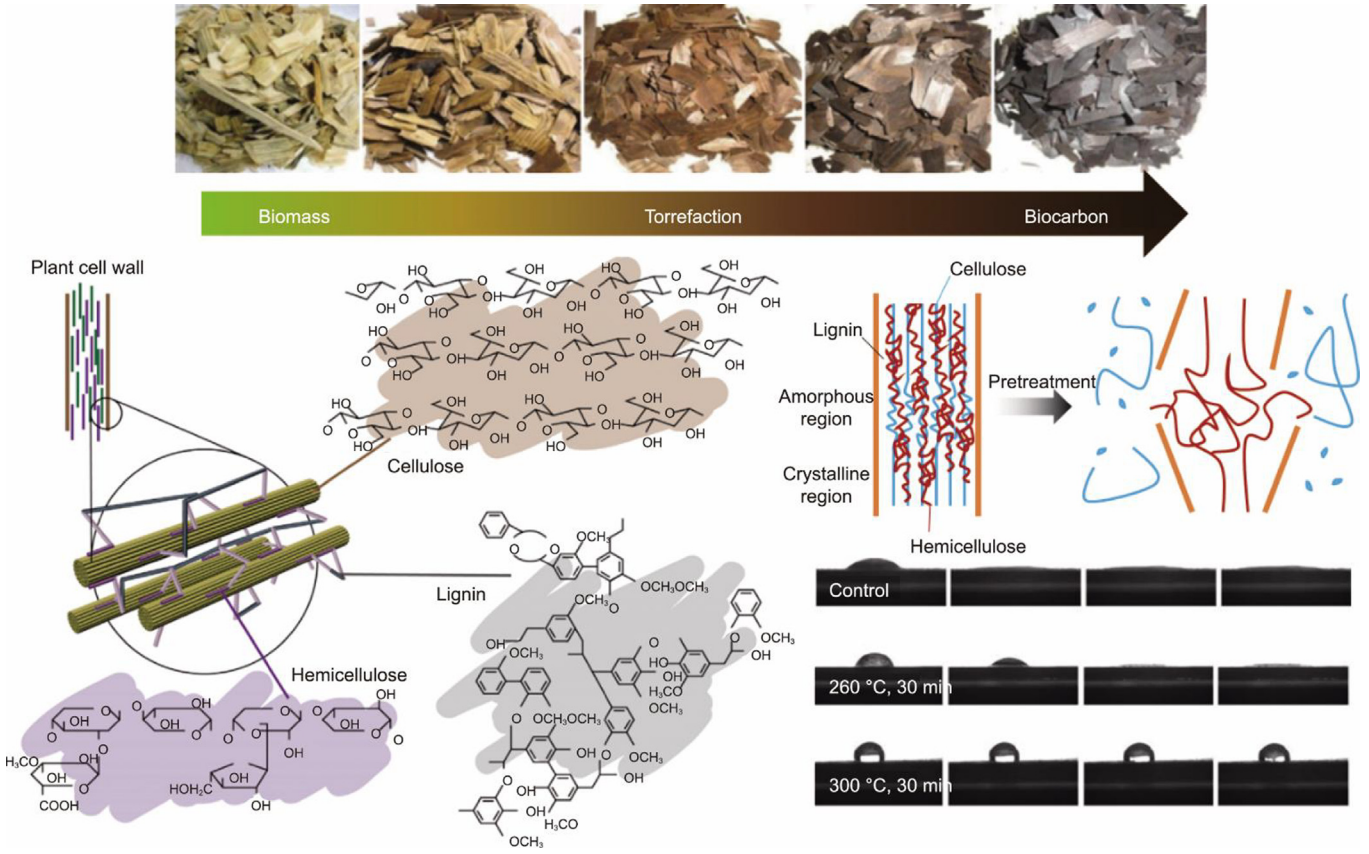

Fig. 2. Biomass characteristics and definition of torrefaction process.

(AAEMs) that contribute to slagging and fouling in high-temperature furnaces.

In this study, ashless kenaf achieved 99.5% potassium removal, reducing unburned carbon (UBC) by 75% and NO_x/SO_x emissions by 43%. These improvements address environmental concerns and enhance combustion stability. In addition, torrefied biomass produced via pyrolysis shows potential as a substitute for coal. Torrefied biomass increases the higher heating value (HHV) from 16.9 to 26.1 $MJ{\cdot}kg^{-1}$, with improved grindability and thermal stability, which is a similar range of thermal coal [26]. Another study on rubberwood-derived biochar reported Hardgrove grindability index (HGI) values similar to those of bituminous coal, confirming its suitability for pulverized fuel injections [27]. Lee et al. [28] also demonstrated that the deposition behavior of ash during combustion is significantly altered by the type of pretreatment, indicating that the choice of the pretreatment directly affects furnace fouling and operational longevity.

Summarily, torrefaction increases energy density but may elevate NO_x emissions, whereas ashless and pyrolytic biochar treatments provide holistic advantages, including reduced slagging potential and improved fuel quality. These technologies lay the foundation for biomass–coal co-firing in PCI systems.

To rigorously evaluate the combustion performance of upgraded biomass fuels under conditions akin to industrial PCI, we utilized three laboratory-scale techniques. ① Laminar flow reactor (LFR): LFR systems reproduce PCI-level flame environments, featuring diffusion-type flat flames at ~26% O_2, peak temperatures of 2000–2250 K, and rapid heating rates (~10^5 $K{\cdot}s^{-1}$). These setups enable detailed observations of ignition delay, volatile combustion, flame structure, particle temperature, fragmentation, and UBC behavior under varying biomass blend ratios. For instance, Kim et al. [29] demonstrated that increasing the biomass share intensifies volatile flame brightness but reduces particle temperatures and fragmentation rates. ② Drop tube furnace (DTF): The DTF offers a cost-effective method for simulating PCI-like combustion, enabling high-temperature, short-residence time testing. It is widely used to assess burnout behavior and often reflects trends similar to those observed in pilot-scale PCI tests. An excellent correlation exists between DTF burnout data and actual PCI performance, validating its reliability for blend evaluation [30,31]. ③ Thermogravimetric analysis (TGA): TGA provides insight into fuel devolatilization, ignition, and burnout kinetics by tracking mass loss with increasing temperature. It is particularly useful for deriving activation energies and combustion indices across various coal and biomass types. For example, Stančin et al. [32] and Zhai et al. [33] used TGA to determine the kinetic parameters of corn stalk and birch pyrolysis, emphasizing its importance for understanding biomass reactivity.

Together, the LFR, DTF, and TGA form a robust analytical suite for characterizing the combustion dynamics of upgraded biomass fuels under PCI-compatible conditions. These methodologies support the development of optimized co-firing strategies by enabling a detailed mapping of blend-dependent ignition and burnout behaviors.

Hydrogen-based ironmaking, which is promising for decarbonization, currently faces critical challenges because of its high cost, supply instability, and storage and transport difficulties. Additionally, the direct use of raw biomass in PCI systems is limited by its low heating value, poor grindability (HGI), and high ash content, making it an impractical direct substitute for PC. In response to these limitations, a stepwise fuel replacement strategy that incrementally introduces upgraded biomass fuels, such as torrefied, carbonized, or ashless biochar, into the PCI process is required. Among these potential routes, the PCI system offers the most technically

feasible and operationally compatible platform for biocarbon integration within existing BF infrastructure. Therefore, this study aims to investigate the combustion behavior and injection limitations of pyrolysis-based biochar within a PCI system, providing a systematic assessment of its potential application. We explore the potential of stepwise biocarbon integration into PCI system as a transitional solution toward carbon-free ironmaking. Specifically, this study has the following objectives: ① Characterizing the combustion behavior of torrefied, carbonized, and ashless biomass; ② analyzing combustion dynamics under varying co-firing ratios; ③ determining the maximum biocarbon injection limit during PCI; ④ assessing the operational and combustion effects of biocarbons on the raceway conditions of a PCI system.

To achieve these goals, combustion behavior was investigated using established thermal analysis (TA) techniques, including TGA, DTF, and LFR. The findings of this study are expected to provide valuable insights for the implementation of stepwise decarbonization strategies in BF ironmaking using biocarbons as a transitional alternative fuel.

2. Analytical and evaluation approaches

2.1. Sample preparation and basic properties of biomass

Five fuel samples were selected to assess their suitability for use in PCI-based ironmaking systems. Commercial PCI-grade bituminous coal (PCI A), which is commonly used in industrial BF operations, was used as the reference coal. In addition, four types of upgraded biomass fuels were used: mildly torrefied biomass (MTB), hard torrefied biomass (HTB), mildly carbonized biomass (MCB), and hard carbonized biomass (HCB). Each biomass sample was thermochemically pretreated the same wood pellet (Table S1 in Appendix A) under inert nitrogen conditions at different temperatures for 1 h to simulate varying degrees of devolatilization and carbon enrichment using LECO TGA 701 (heating rate was 20 K·min^{-1} up to each treating temperature): MTB (573 K for 1 h under N_2 (mild torrefaction)); HTB (673 K for 1 h under N_2 (hard torrefaction)); MCB (773 K for 1 h under N_2 (mild carbonization)); HCB (1073 K for 1 h under N_2 (hard carbonization)).

All samples were ground to a particle size between 75 and 90 μm, consistent with the standard PCI input particle range. To minimize the influence of moisture, all materials were pre-dried by placing them in an open atmosphere at 40 °C for 24 h before analysis. Basic fuel properties, including moisture, volatile matter, ash, and fixed carbon content, were determined through proximate analysis using a thermogravimetric analyzer (TGA 01, LECO Co., USA) following American Society for Testing and Materials (ASTM) standards [34–37]. Ultimate analysis was performed using a CHNS analyzer (Leco-TruSpec Micro CHNS, LECO Co.) to quantify the carbon, hydrogen, nitrogen, and sulfur contents, following ASTM D5373 [38]. Infrared spectroscopy was used to detect carbon, hydrogen, and sulfur, and nitrogen was measured using thermal conductivity. The oxygen content was calculated based on the difference. The calorific value (HHV) was determined using an adiabatic bomb calorimeter (5E-C5500 Automatic Calorimeter, Changsha Kaiyuan Instruments Co., China) following ASTM D5865 [39]. Each dried sample was combusted in a pressurized oxygen atmosphere, and the HHV was calculated from the observed temperature increase in water.

Additionally, elemental ratios, such as H/C and O/C, were calculated from the ultimate analysis results to evaluate the degree of aromatization and devolatilization. Vitrinite reflectance analysis was conducted for PCI coal A (Details of vitrinite reflectance results show in Fig. S1 in Appendix A). These parameters are widely recognized as key indicators for fuel upgrading [40]. The basic fuel properties are summarized in Table 1. The relatively higher moisture content of HCB is attributed to increased pore development after carbonization, which promotes moisture adsorption. (Fig. S2 in Appendix A)

2.2. Fixed bed combustion characteristics with TGA

A thermogravimetric analyzer was used to measure the mass change in the samples as a function of temperature, enabling the analysis of pyrolysis behavior and thermal stability. By observing the rate and stages of decomposition, the TGA provides insights into the reaction mechanisms of solid fuels. In this study, an SDT-Q600 model from TA Instruments was used for TGA measurements.

The samples analyzed included PCI A, MTB, HTB, MCB, and HCB, which were ground and sieved to a uniform particle size within the range of 75–90 μm. The sample mass was fixed at 20 mg for the PCI A, MTB, HTB, MCB, and HCB. To minimize moisture influence, all samples were dried under air-dried basis conditions by placing them in an air atmosphere at 313 K for 24 h. To analyze single-fuel combustion characteristics, the tests were conducted under an air atmosphere (N_2 79.0 vol%, O_2 21.0 vol%) with a gas flow rate of 100 mL·min^{-1}. The heating rate was set to 5 K·min^{-1}, ramping up to 1323 K, and the temperature was maintained for 10 min before cooling under ambient conditions. The experimental conditions are listed in Table 2. TGA experiments were performed 5 times for each case, and the average was used to discuss results. Thermogravimetric and derivative thermogravimetric (DTG) curves were calculated and used for kinetic analysis. The Coats–Redfern integral method was employed to linearize the thermogravimetric data. The activation energy (E_a) and pre-exponential factor (A) were determined from the slope and intercept of the fitted line, respectively.

Before kinetic calculations, the extent of a reaction is defined using the following equation:

$$x(t) = \frac{w_0 - w(t)}{w_0 - w_f} \tag{1}$$

where w_0 is the initial weight, w_f is the weight after reaction, x represents the conversion rate, and t denotes time. Therefore, the extent of the reaction over time can be calculated by converting the measured mass-loss data. The kinetic constant can be derived from the reaction rate, which corresponds to the time derivative of the conversion rate. The fundamental equations are as follows:

$$\frac{dx}{dt} = k \cdot f(x) \tag{2}$$

$$k = A \cdot \exp\left(-\frac{E_a}{RT}\right) \tag{3}$$

$$\frac{dx}{dt} = A \cdot \exp\left(-\frac{E_a}{RT}\right) \cdot f(x) \tag{4}$$

where k is the kinetic constant, $f(x)$ is the differential conversion function, R is the universal gas constant, and T is the absolute temperature. At a constant heating rate, the equation can be transformed as follows:

$$\frac{dx}{dt} = \frac{dx}{dT}\frac{dT}{dt} = \frac{dx}{dT} \cdot \beta = A \cdot \exp\left(-\frac{E_a}{RT}\right) \cdot f(x) \tag{5}$$

$$\frac{dx}{dT} = \frac{A}{\beta}\exp\left(-\frac{E_a}{RT}\right) \cdot f(x) \tag{6}$$

where β represents the heating rate, $f(x)$ is commonly expressed as $(1-x)^n$, and x is conversion ratio of samples. In this study, n is

Table 1
Sample properties analysis (proximate, ultimate, calorific, and vitrinite-reflectance analysis).

Analysis	PCI A	Torrefaction biomass		Carbonization biomass	
		MTB	HTB	MCB	HCB
Proximate analysis (air dry basis, wt%)					
Inherent moisture	1.01	1.74	1.83	1.63	6.84
Volatile matter	15.27	51.14	17.81	16.50	9.54
Fixed carbon	73.83	45.60	78.93	80.98	68.73
Ash	9.90	1.52	1.43	0.89	14.89
Ultimate analysis (dry and ash-free basis, wt%)					
C	88.870	69.51	87.93	87.92	92.62
H	4.420	4.78	2.79	2.64	1.57
N	1.890	0.23	0.51	0.43	0.8
O	4.310	25.46	8.74	8.97	4.88
S	0.510	0.02	0.03	0.04	0.13
Vitrinite reflectance (%)	0.709	–	–	–	–
Atomic ratio					
H/C	0.5968	0.8252	0.3808	0.3603	0.2034
O/C	0.0364	0.2747	0.0745	0.0765	0.0395
Calorific properties ($MJ \cdot kg^{-1}$)					
HHV	31.766	26.279	31.891	32.331	25.796

Table 2
Experimental conditions of TGA.

Parameter	Condition
Particle size	75–90 μm
Temperature	5 $K \cdot min^{-1}$ to 1323 K
Selected gas	Air (N_2 79.0 vol%, O_2 21.0 vol%)
Flow rate	100 $mL \cdot min^{-1}$

assumed to be 1, which is a typical simplification. Accordingly, the equation can be revised as

$$\frac{dx}{dT} = \frac{A}{\beta}\exp\left(-\frac{E_a}{RT}\right) \cdot (1-x) \tag{7}$$

By dividing both sides of the equation by $(1-x)$ and taking the natural logarithm, the expression can be rearranged as follows:

$$\frac{dx}{dT}\frac{1}{1-x} = \frac{A}{\beta}\exp\left(-\frac{E_a}{RT}\right) \tag{8}$$

$$\ln\left(\frac{dx}{dT}\frac{1}{1-x}\right) = \ln\left(\frac{A}{\beta}\right) - \frac{E_a}{RT} \tag{9}$$

In this study, a first-order reaction model, $f(x) = (1-x)$, was applied uniformly to all samples to ensure consistent comparison of activation energy and pre-exponential factors. This simplified mechanism is commonly adopted in biomass and coal combustion studies and enables direct evaluation of relative combustion reactivity based on the conversion–temperature profiles.

2.3. Dynamic combustion characteristics analysis with DTF

The combustion behavior of the samples was investigated using a DTF system (Fig. 3) consisting of injection, reaction, and collection modules. To ensure a consistent comparison across samples, all fuels were tested under the following uniform conditions: gas flow rate, temperature, and residence time.

The injection system comprised a vibrator, syringe pump, and double-tube assembly, designed to steadily deliver pulverized fuel into the reactor. The gap between the feed tube and particle reservoir was carefully maintained to ensure stable feed rates. A mass-flow controller regulated the flow of carrier and reaction gases over the duration of the test. The reactor zone was heated to 1800 K to

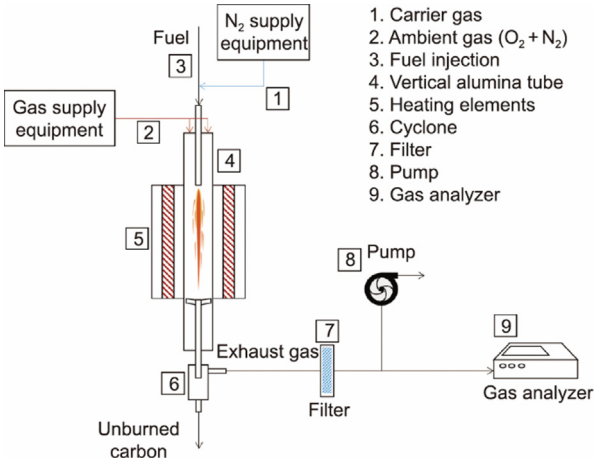

Fig. 3. Schematic of DTF.

simulate combustion environments relevant to PCI operations. The system provides extremely fast heating rates on the order of 10^4–10^5 $K \cdot s^{-1}$, closely resembling the thermal conditions in BF injection systems [7]. The length of the high-temperature reaction zone was adjusted 50–200 mm, depending on the experimental requirements.

After combustion, UBC was collected using a cooling-integrated unit comprising a sampling probe, cyclone, and filter holder. Continuous water cooling was applied to prevent secondary reactions after sampling. Although actual PCI operations often involve preheated air and oxygen-enriched environments, the DTF setup employed ambient air because of limitations in hot-air feeding capabilities. The oxygen concentrations were selected to mimic the BF operating conditions. In the previous research [41], despite the variation in oxygen enriched condition (21.0–26.0 vol%) in PCI-like tests, the relative burnout trends among different fuels remain consistent, indicating that a DTF experiment conducted at 21 vol% O_2 is sufficiently representative for comparing combustion behavior. Detail conditions of DTF experiments are presented in Table 3.

To assess combustibility, the UBC content was quantified using an ash tracer method, as shown in Eq. (10) [7]:

Table 3
DTF experimental conditions for BF.

DTF Parameter	BF
Experiment temperature (K)	1573
Sample particle size (μm)	75–90
Coal feeding rate ($g \cdot min^{-1}$)	0.3
Total gas flow ($L \cdot min^{-1}$)	5
Residence time (s)	0.75
Oxygen concentration (vol%)	21.0

$$\mathrm{UBC}(\%) = \left[\frac{A_0(100 - A_{\mathrm{char}})}{A_{\mathrm{char}}(100 - A_0)}\right] \times 100 \quad (10)$$

where A_0 and A_{char} are the ash contents of the original fuel and collected char, respectively. The derived UBC values were used to analyze the relationship between fuel blend ratio and combustion efficiency in PCI dynamic system. Also, the DTF experiments were performed 5 times for each case, and average of UBC was used to discuss results.

2.4. Analysis of biomass contribution in UBC after co-firing

To evaluate the contribution of biomass to the UBC content in co-firing experiments, radiocarbon dating was employed to quantify the proportion of biomass-derived carbon remaining in the collected UBC. The analysis was conducted by a certified laboratory specialized in radiocarbon measurements (Carbon Analysis Lab Co., Ltd.). The procedure was as follows: approximately 5–10 mg of the collected UBC sample was dried, pulverized, and purified using chemical or physical methods to eliminate impurities.

Then, the refined sample was combusted in an elemental analyzer (EA) to convert all carbon into CO_2. The evolved CO_2 was captured and subsequently reduced to graphite in a carbon reduction furnace.

The graphite was mounted onto the sample target of an accelerator mass spectrometer, where the ionized carbon beam was separated by mass, and the $^{14}C/^{12}C$ ratio was precisely measured. This radiocarbon ratio is used to differentiate between fossil-derived carbon (e.g., PCI coal) and modern carbon (e.g., biocarbon) in a sample [42,43]. Using this approach, the biomass-derived fraction of UBC in the DTF co-firing tests was quantitatively determined and compared across the test conditions.

2.5. Observation of flame behavior using LFR

In this study, the ignition delay and char combustion behavior of each fuel type were evaluated through direct visualization using an LFR system [44,45]. This apparatus generates a laminar diffusion flame over a flat burner, providing a controlled high-temperature environment for observing coal particle ignition and subsequent flame dynamics.

The combustion behavior of the injected fuels in the LFR was analyzed using charge-coupled device (CCD)-based flame imaging. Approximately 200 images were acquired for each test, and a subset of representative frames was used to construct time-averaged images. The average images were converted to grayscale (0–255 intensity range), and the ignition onset position was defined at 50% of the maximum intensity threshold. Based on the spatial distribution of intensity along the particle trajectory, the ignition delay region, volatile combustion cloud, and char combustion zone were distinguished. The pixel-to-length calibration enabled quantitative extraction of ignition delay length and char combustion length, allowing direct comparison of combustion characteristics among the biocarbon samples. A schematic of the system and image processing method are shown in Fig. 4.

The LFR setup includes a flat-flame burner, gas supply system, and fine coal feeding unit, all mounted on a two-axis positioning platform. The burner uses a stainless-steel capillary honeycomb to generate a flat laminar diffusion flame, with the post-flame oxygen maintained at 21% to simulate ambient air. A rectangular quartz tube stabilizes the flame during operation. Consistent feeding of PC (<100 μm) is challenging due to electrostatic effects; therefore, a custom syringe-based feeding system with a vibrator and syringe pump was developed. The actual feed rate was verified by measuring the mass of coal delivered over time to ensure a stable fuel supply [45].

The supplied gases were categorized based on their functions: either for flat flame generation (fuel and oxidizer) or coal particle transport. The burner design allows for flexible adjustment of the fuel–oxidizer mixture to achieve the desired combustion atmosphere required for burning coal particles. Each gas stream was regulated using a dedicated mass flow controller (MFC), with all MFCs integrated into a centralized control interface for precise flow management. Carbon monoxide and hydrogen served as primary fuels to produce a flat laminar flame, and nitrogen was used to dilute concentrations and serve as a carrier gas during coal injection. Oxygen and nitrogen were used as oxidants to establish specific combustion atmospheres. The flow conditions for each gas stream are listed in Table 4. PC particles were injected into the flat flame under 21% O_2 (ambient air), which simulated the BF and BF PCI environments. Under these conditions, the flat flame exhibited peak temperatures between 2000 and 2250 K [45].

To validate the applicability of the LFR in PCI-related studies, Lee et al. [45] performed a conceptual comparison between the LFR setup and a real BF tuyere system. In both systems, finely pulverized fuel was injected through a lance, forming a flame zone known as raceway. In the LFR, the premixed gases form a flat diffusion flame, into which pulverized fuel is introduced, closely mimicking the raceway behavior in actual PCI operations. Therefore, the LFR apparatus effectively replicated the flame formation zone of PCI systems, justifying its use in this study. Thus, the combustion mechanism of PC was visualized and analyzed with a focus on the injection region to simulate raceway phenomena under controlled laboratory conditions [45].

2.6. Maximum injection limit of biocarbon in PCI

The BF has been continuously improved to enhance productivity and reduce operating costs. Particularly, efforts to increase productivity and reduce coke and fuel consumption in steel plants are being pursued to maintain competitiveness in the global steel market. One representative improvement strategy involves a shift in fuel sources. Conventionally, petroleum has been the primary fuel used in BFs. However, rising international oil prices have led to a decline in cost competitiveness, prompting the exploration of alternative fuels. Natural gas and coal, which are abundant, widely distributed, and easier to manage, have been proposed as substitutes. Currently, most steel plants employ PCI technology and use coal as the main fuel. Although the initial adoption of coal was driven by high oil prices, increasing PCI rates today are motivated by the need to reduce raw material costs and lower air pollutant emissions.

The application of PCI in BFs offers the following advantages [46]: it improves furnace productivity, that is, the quantity of hot metal produced by the BF; it allows the substitution of expensive coke with cheaper coke or steam coal, thereby reducing the coke consumption and associated costs; it helps maintain furnace stability; it enhances the quality of the hot metal and reduces the silicon content in pig iron. An increase in the PCI rate can result in up to a 6.7% reduction in CO_2 emissions.

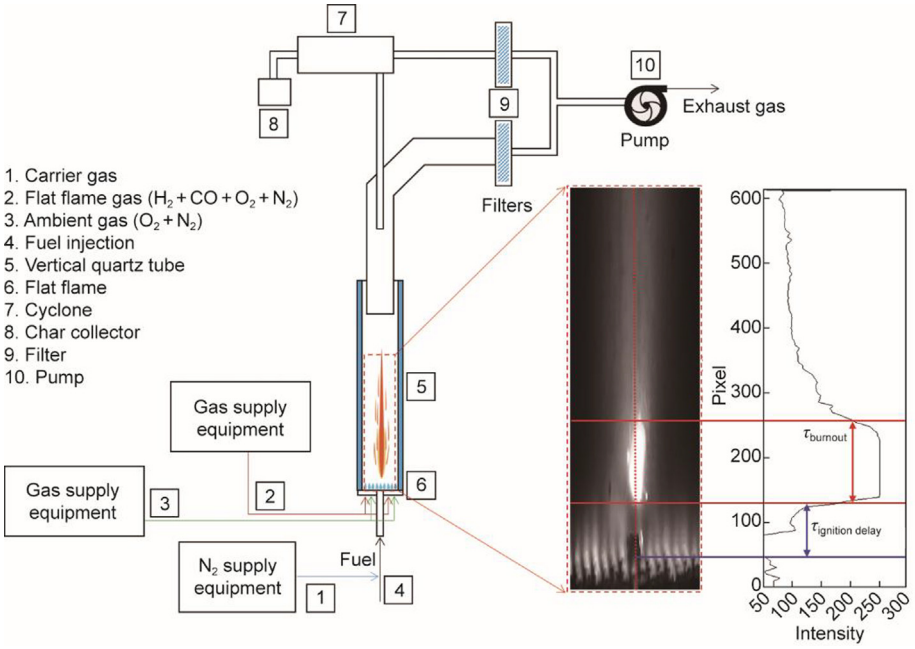

Fig. 4. Schematics of LFR and image processing method. $\tau_{burnout}$: time for burnout; $\tau_{ignition\ delay}$: time for ignition delay.

Table 4
Experimental condition of LFR.

Condition	Actual flow rate (SLPM; L·min^{-1})
O_2 21% (BF)	
N_2 (que)	15
N_2 (car)	0.367
Fuel	
CO	3.04
H_2	0.74
N_2	2.64
Oxidizer	
O_2	6.20
N_2	3.54

Due to these benefits, efforts to increase PCI rates continue to pursue enhanced productivity and cost savings through reduced coke usage. This has led to the development of technologies for coal pulverization, storage, and transport. In addition, innovations such as uniform coal distribution in the tuyeres, lance design optimization, and oxygen enrichment control for combustion regulation have been actively developed.

A correlation between PCI and coke rates has been demonstrated, indicating that as the PCI rate increases, the coke rate decreases. Thus, higher PCI injection rates are directly related to cost reduction. Fig. 5 illustrates the phenomena occurring at the tuyere as the PCI rate of high-volatile coal increases. This observation is similar to that of biocarbons [47]. Generally, as the carbon content of PCI coal increases up to approximately 91% on a dry ash-free (daf) basis, the coke replacement ratio increases. However, beyond this point, further increases in carbon content do not lead to additional replacement benefits. Moreover, when the carbon content exceeds 85% (daf), the blast momentum decreases; this finding is closely related to the depth of the raceway. In such cases, oxygen-enriched operations can be used to maintain combustion temperature. The findings illustrated in Fig. 5 indicate that increasing the injection rate of high-volatile coals increases blast pressure and momentum, resulting in an enlarged and unstable raceway zone. This instability is accompanied by the increased formation of fine coke particles, potentially affecting the furnace stability and overall productivity. Nonetheless, when assessing the maximum allowable PCI rate, the foremost factor to be considered is system capacity. As previously mentioned, evaluating whether parameters such as pulverizer throughput, excess air supply, preheated air temperature, and ash-handling capacity inside the BF fall within the feasible injection limits is necessary.

The theoretical air requirement, dry flue gas volume, and combustion-generated water vapor can be calculated using the ultimate analysis of the fuel, typically represented by the elemental composition (C, H, O, S, and N). These parameters are essential for evaluating the combustion burden imposed on the BF system and serve as the foundation for determining the maximum injection limit of pulverized fuels in PCI.

Theoretical air requirement:

$$\mathrm{Air_{th}} = 0.0889 \times M_C + 0.2667 \times M_H + 0.0333 \times M_S - 0.0333 \times M_O \quad (11)$$

Theoretical dry flue gas volume:

$$\mathrm{Gas_{dry}} = 0.0187 \times M_C + 0.0667 \times M_H + 0.0187 \times M_S - 0.0071 \times M_O \quad (12)$$

Combustion-generated water vapor:

$$\mathrm{H_2O_{vapor}} = 0.623 \times M_H \quad (13)$$

Here, M_C, M_H, M_O, M_N, and M_S are the mass fractions (kg·kg^{-1} of fuel) obtained from the ultimate analysis. All constants are derived from stoichiometric combustion equations under standard conditions (0 °C, 10^5 Pa). The flue gas volume per unit of fuel is estimated based on the theoretical combustion outputs. By comparing the total flue gas generated at various injection rates with the gas handling and ash processing capacities of the furnace, the maximum feasible injection limit of each fuel can be determined. This approach ensures stable raceway operation, minimizes overburden on the blower system, and avoids excessive slagging due to ash content.

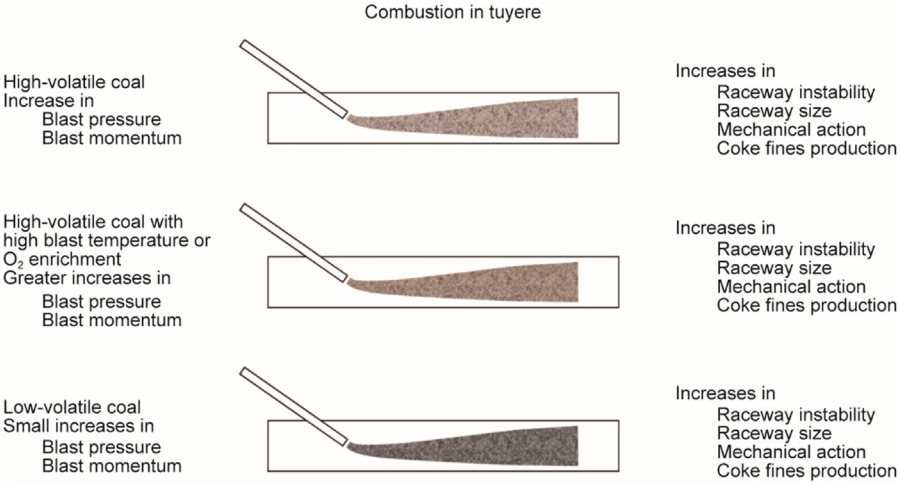

Fig. 5. Combustion mechanism of high-volatile coal in tuyere.

3. Experimental results and discussion

3.1. Combustion kinetics of biocarbon

TGA was performed to evaluate the combustion characteristics of PCI coal and upgraded biomass fuels (MTB, HTB, MCB, and HCB). TG and DTG curves were used to assess mass loss and reaction rates at different temperatures. Each sample exhibited characteristic combustion behavior, including ignition temperature, peak reactivity, and residual ash. Biomass samples generally showed lower ash residues and earlier ignition than coal, whereas carbonized samples demonstrated higher reaction rates. These observations reflect the effect of thermal treatment on combustion dynamics.

As shown in Fig. S3 in Appendix A, PCI coal exhibited a typical two-stage combustion profile with an initial moisture loss and a slight mass increase due to oxygen adsorption. The main combustion phase occurred between 714.3 and 847.6 K, with a peak reaction rate of 4.862% min^{-1} at 789.3 K and 8.21% ash residue. MTB displayed two distinct DTG peaks at 581.6 and 705.7 K, indicating separate devolatilization and char combustion phases, with a minimal ash content of 1.52%. HTB, which was treated at a higher temperature, exhibited combustion from 636.4 to 775.6 K and a peak reactivity of 5.124% min^{-1}. Further carbonization increased the combustion intensity. MCB reacted between 635.6 and 773.4 K with a peak DTG of 5.313% min^{-1} and the lowest ash residue (0.89%), indicating complete combustion. Despite having the highest ash content (14.89%), HCB exhibited the fastest reaction (6.651% min^{-1} at 713.7 K), probably because of the increased fixed carbon concentration and structural modification during high-temperature carbonization. These results show the influence of pretreatment temperature on fuel reactivity and burnout behavior.

The reaction rate and temperature data derived from the TG/DTG curves were used to calculate kinetic parameters using the Coats–Redfern method. The results are illustrated in Fig. 6 and Table 5. The activation energy (E_a) of PCI coal was 1.4353×10^5 kJ·$kmol^{-1}$, serving as a baseline for comparing the single-combustion characteristics of biocarbons. For biocarbons, E_a ranged from 6.706×10^4 to 1.5890×10^5 kJ·$kmol^{-1}$, which is generally lower than that of the other samples. This indicates that biocarbons are less thermally stable and can initiate reactions at relatively low energy thresholds. Notably, MTB exhibited the lowest E_a (6.706×10^4 kJ·$kmol^{-1}$), probably because of its low degree of carbonization and remaining volatile content. The pre-exponential factor (A) of biocarbon ranged from 0.193×10^3 to 5.275×10^8 s^{-1}, indicating that although thermal stability increases with higher pretreatment temperatures, once ignition occurs, the reaction proceeds more rapidly. The Coats–Redfern kinetic fitting showed high agreement with the experimental data, with R^2 values of 0.9938, 0.8993, 0.9920, 0.9992, and 0.9621 for PCI A, MTB, HTB, MCB, and HCB, respectively.

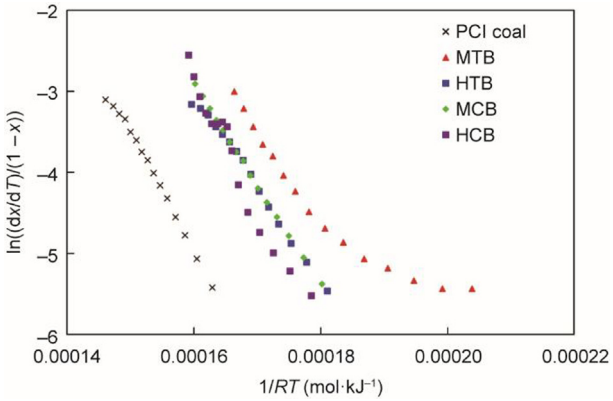

Fig. 6. Kinetic analysis of each sample using the Coats–Redfern method.

Table 5
Activation energy and pre-exponential factors of each sample.

Sample	Kinetic constant	
	E_a ($\times 10^4$ kJ·$kmol^{-1}$)	A ($\times 10^3$ s^{-1})
PCI coal	14.353	5517.221
MTB	6.706	0.193
HTB	11.479	374.919
MCB	12.471	2115.829
HCB	15.890	5.275×10^5

3.2. Co-firing combustibility of biocarbon

The results of the co-firing combustion tests on the PCI coal and biocarbon samples (MTB, HTB, MCB, and HCB) are presented in Figs. S4(a)–(d) in Appendix A. At a blending ratio of 3%, MTB, HTB, and MCB exhibited a slight reduction in combustibility, as indicated by the increased UBC compared with that of only PCI coal. Despite the higher intrinsic combustibility of the biocarbon samples, this early-stage blending led to less favorable combustion. As the blending ratio increased to 5%, combustion

performance generally improved, especially in HTB and MCB, with UBC values comparable to those of PCI coal. For MTB, combustion improved further by 10%, exceeding the performance of the single-coal case. However, MCB at 10% blending still exhibited slightly lower combustibility than HTB, probably because of its moderate devolatilization characteristics.

HCB, which underwent the highest heat treatment, exhibited the most consistent improvement in combustion with increasing blending ratio (Fig. S4(e) in Appendix A). Its UBC values decreased steadily from 3% to 10% blending, outperforming PCI coal at all levels. This trend shows that the higher thermal stability and fixed carbon content of HCB contribute significantly to its better combustion behavior. Overall, although the low-ratio blending of biocarbons may initially hinder combustion because of particle interaction or flame instability, higher ratios, particularly with more thermally treated samples, enhance performance and demonstrate potential for use in co-firing strategies.

Fig. 7 illustrates the UBC composition results based on radiocarbon dating, showing the respective contributions of PCI coal and biocarbons in the collected UBC. For MTB, more than 99% of the UBC originated from coal, with a slight increase in the overall UBC as the blending ratio increased. This is probably owing to the high reactivity of MTB, which retains significant biomass characteristics, as it is produced at a relatively low treatment temperature (300 °C), allowing most of the biocarbons to combust completely. For HTB, biocarbon-derived UBC accounted for approximately 1% at a blending ratio of 3%, decreased to 0.43% at 5%, and increased to 2.06% at 10%. MCB exhibited a similar trend: at 3% blending, biocarbon-derived UBC was 0.53%, which decreased to 0.16% at 5%, and then rose again to 0.39% at 10%. For HCB, the overall UBC decreased with an increasing blending ratio, indicating that most of the injected HCB was combusted. Therefore, radiocarbon analysis was not conducted for HCB.

The co-firing behavior observed in the DTF experiments can be interpreted in relation to general solid-fuel combustion mechanisms. In pulverized fuel combustion, the ignition and early flame development are primarily governed by volatile release, whereas the subsequent char burnout stage is controlled by the fixed-carbon structure and the accessibility of oxidizing gases to internal reaction sites. Accordingly, samples with relatively high volatile content, such as MTB, exhibited increased UBC at low blending ratios because rapid devolatilization can induce transient flame instability. As the carbonization severity increased (HTB → MCB → HCB), structural ordering of the carbon matrix and the development of internal pore networks enhanced oxygen diffusion and char oxidation, which is consistent with the progressive reduction in UBC at higher blending ratios. Although ash is generally associated with the formation of surface diffusion barriers that hinder gas–solid contact, the highly carbonized HCB showed continuously improved burnout performance. This behavior is attributed to particle fragmentation during combustion, which exposes fresh reactive surfaces and mitigates ash-induced mass transfer resistance; the fragmentation mechanism and its influence on flame structure are discussed in detail in Section 3.3. Therefore, the co-firing combustibility trends are governed by the combined effects of volatile-driven ignition characteristics, fixed-carbon burnout reactivity, and the degree to which ash accumulation is counteracted by fragmentation-induced pore exposure during char oxidation.

3.3. Combustion mechanism identification with PCI flame visualization

LFR experiments were conducted to visually investigate the combustion characteristics of PCI coal and each biocarbon (MTB, HTB, MCB, and HCB) under single- and co-firing conditions. The analysis focused on ignition delay, char combustion length, fragmentation, and formation of flame clouds.

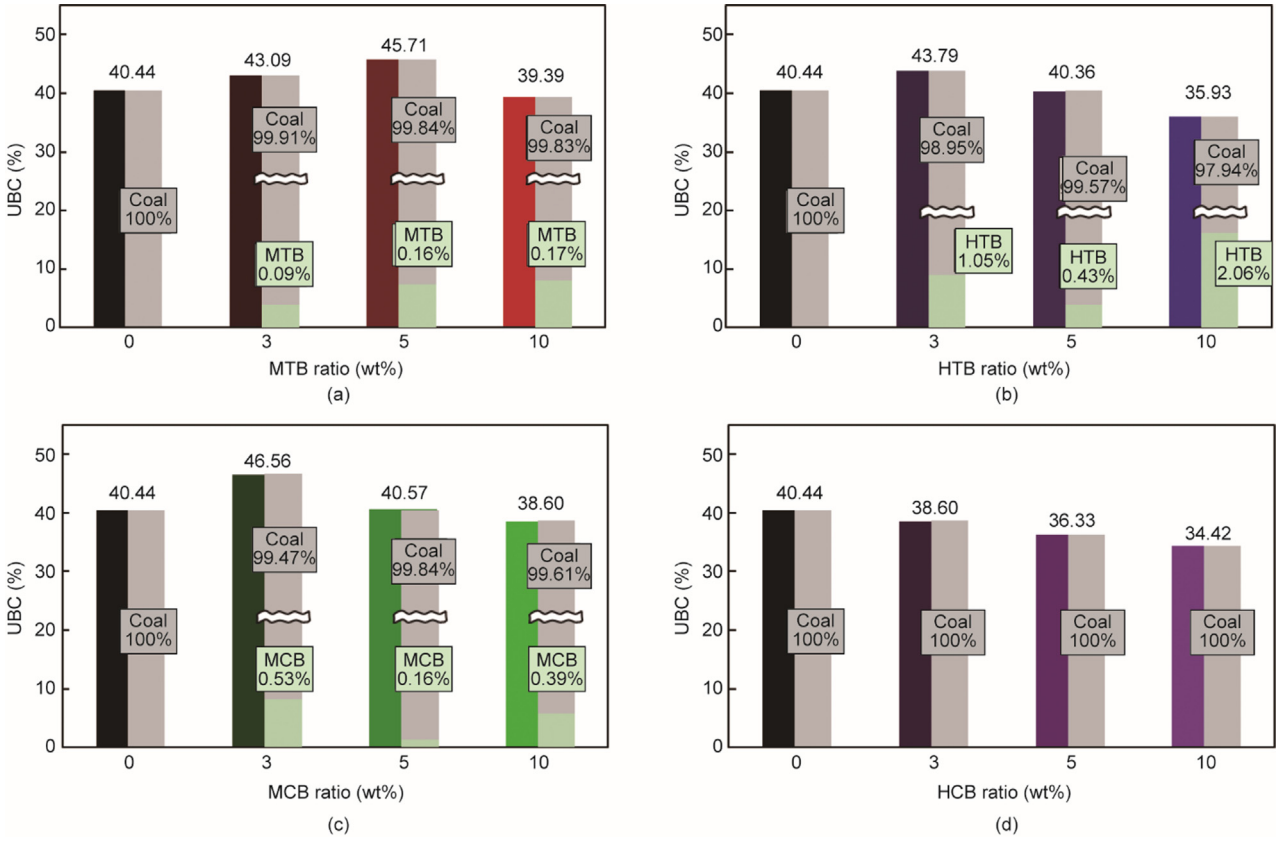

Fig. 7. UBC blended ratio of PCI coal and (a) MTB, (b) HTB, (c) MCB, and (d) HCB.

In co-firing experiments, for MTB, increasing the blending ratio led to larger flame cloud areas, reduced fragmentation, and extended combustion lengths. However, due to its high reactivity, the overall combustion length under co-firing was still shorter than that of PCI coal. For HTB and MCB, the combustion length decreased to 3% co-firing but increased to 5% and above owing to intensified fragmentation, which also contributed to a longer ignition delay. When fragmentation occurred, the resulting coal and biocarbon particles tended to fragment along the laminar flow direction because of the conservation of internal momentum within the coal structure. Consequently, the particle velocities increased, leading to an extended trajectory. This phenomenon contributed to a longer combustion path, thereby increasing the overall char combustion length. Despite this observation, the DTF results showed a decrease in UBC, indicating improved overall combustibility. For HCB, both flame brightness and cloud formation increased with blending ratio, and combustion length was extended owing to its lower heating value.

Overall, MTB is most suitable for co-firing at up to 3%, whereas HTB and MCB can be effectively co-fired at 5% or higher without deteriorating combustion performance. HCB, because of its lower heating value, may increase the total fuel input under high co-firing ratios and thus requires careful optimization. All visual results are illustrated in Fig. 8.

The combustion mechanism within the PCI system was clarified based on previous DTF and LFR experimental results, as illustrated in Fig. 9. For MTB, the UBC increased up to a co-firing ratio of 5% but decreased below that of coal alone at 10%. This behavior is attributed to the competing effects of char combustion enhancement due to coal fragmentation and the high volatile content and intrinsic combustibility of biocarbons. Notably, MTB exhibited significantly higher volatile matter content than other biocarbons, leading to early combustion of volatiles and thus shifting the inflection point to a relatively higher co-firing ratio.

For HTB and MCB, unlike MTB, the dominant effect was combustion enhancement due to biocarbon fragmentation rather than volatile combustion. Consequently, the inflection point appeared earlier than expected, at a co-firing ratio of 3%, and the UBC continued to decrease with a further increase in the co-firing ratio. For HCB, both coal and biocarbons exhibited active fragmentation, resulting in a consistent reduction in UBC as the co-firing ratio increased. This trend shows that the moderate volatile content and high fragmentation behavior of HCB contribute to improved combustion performance.

3.4. Maximum injection limit evaluation of biocarbon

Among steelmaking processes, the ironmaking stage accounts for approximately 82% of the total carbon emissions, rendering it the primary target for decarbonization. Global strategies to achieve carbon neutrality include transitioning from conventional BF operations to EAF and utilizing hydrogen and biomass as alternative fuels. As a transitional solution, replacing PCI coal with biocarbons has emerged as a viable, low-carbon bridge technology. This study quantitatively evaluates the applicability and injection limitations of biocarbon materials (MTB, HTB, MCB, and HCB) as substitutes for PCI coal in a BF-PCI system. To determine the maximum feasible injection rates, the operational conditions of the BF and the physicochemical and combustion properties of the biocarbon samples were considered. As presented in Table 6, the baseline BF operation was set to 500 kg·tHM^{-1} (here HM refers hot metal) of the total injected fuel, comprising 350 kg·tHM^{-1} of coke and 150 kg·tHM^{-1} of PCI coal [48]. In this study, the coke input remained fixed while PCI coal was partially substituted with biocarbons. Combustion behavior derived from the DTF and LFR experiments was used to determine suitable blending ratios. The calorific value was restricted to within ±5% of PCI coal, and the total ash content after blending was limited to below 10%. Table 7 presents the calculated

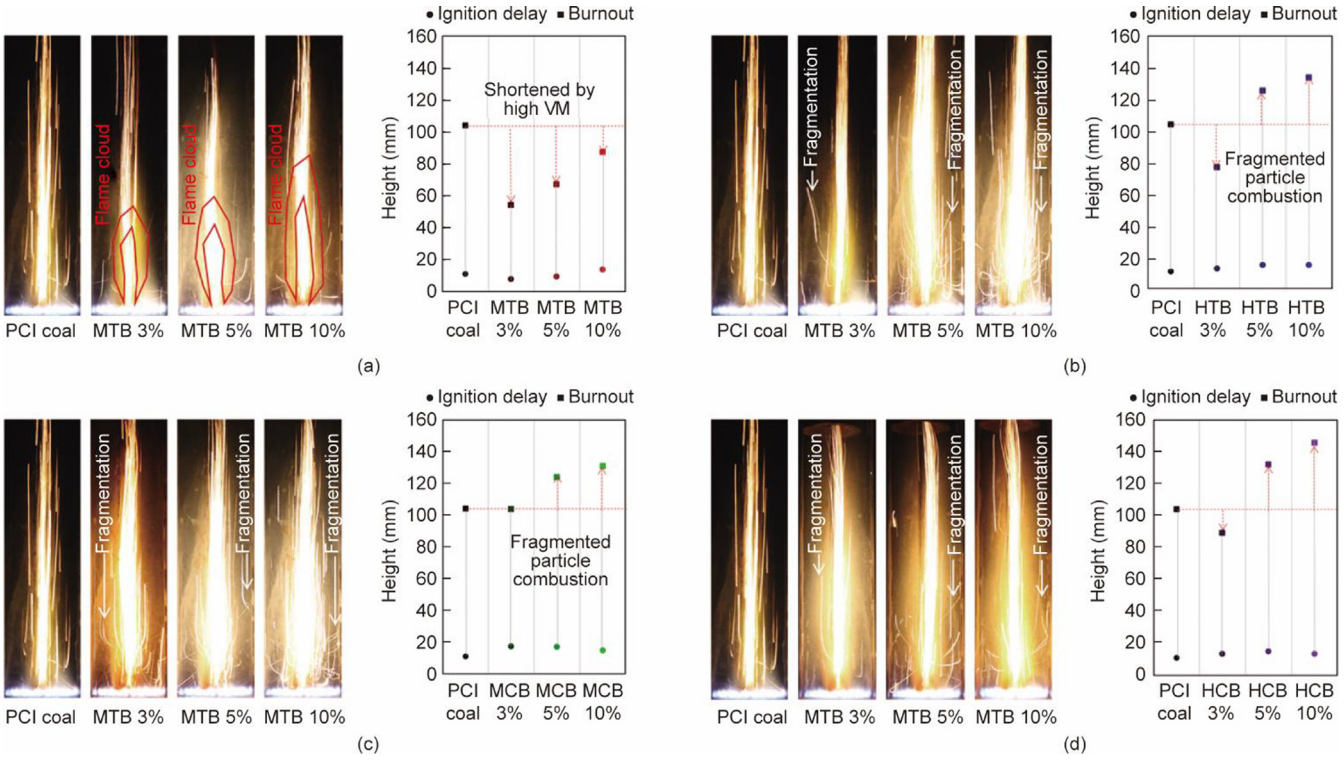

Fig. 8. Flame visualization of (a) MTB, (b) HTB, (c) MCB, and (d) HCB on co-firing with PCI coal (maximum intensity of 20 images for each case).

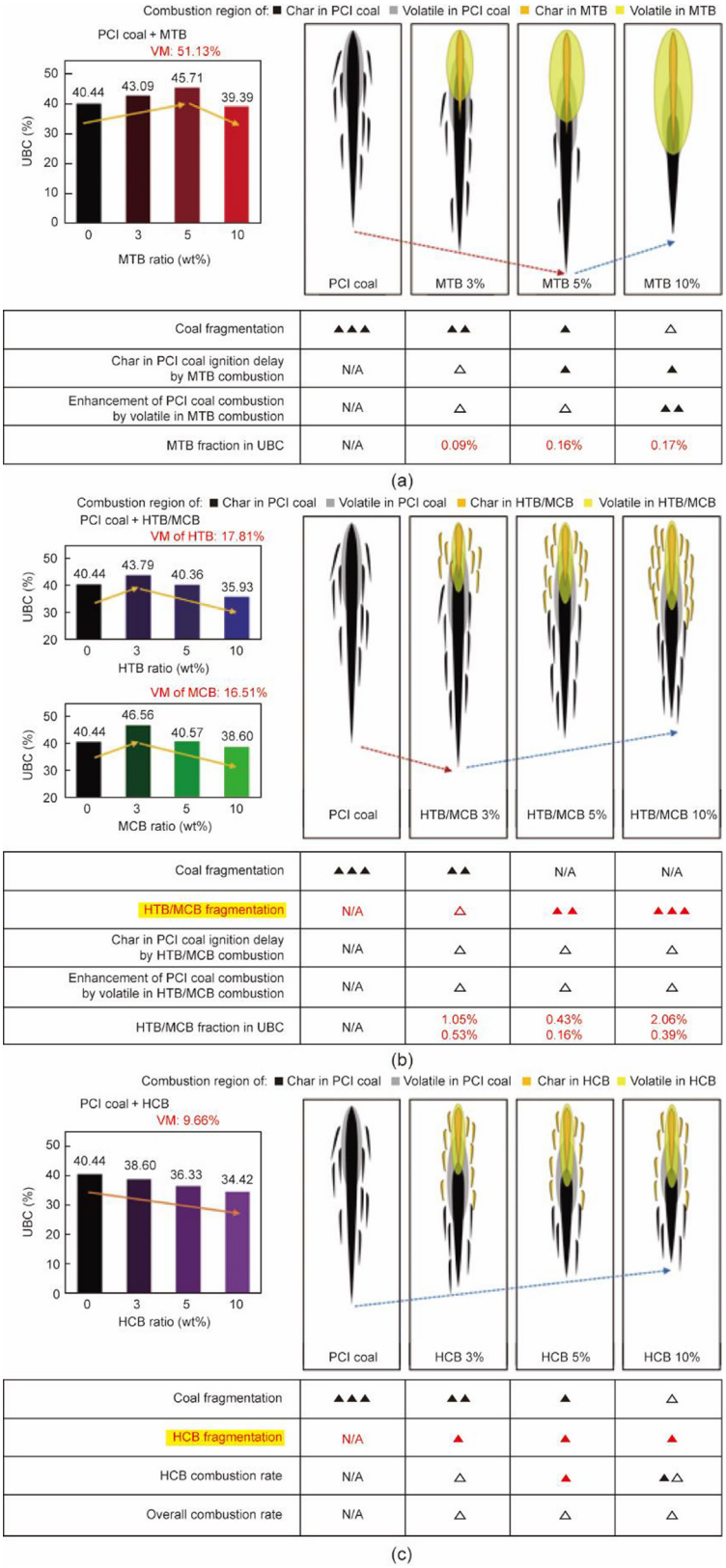

Fig. 9. Combustion mechanism of coal and (a) MTB, (b) HTB, and (c) co-firing with LFR.

optimal injection limits for each sample, and Fig. 10 shows graphs derived from a numerical evaluation of the heating value and ash content constraints. The HHV and ash content of the blended fuels were calculated based on the mass mixing ratio of PCI coal and biocarbon. The maximum injection limits were determined by identifying the blending level at which the mixed HHV remained within ±5% of PCI coal and the total ash content did not exceed 10 wt%. MTB and HCB exhibited lower calorific values, exceeding the

Table 6
Operation target of the BF.

Indices	Design
Production	2.0 Mt·a^{-1}, 5500 t·d^{-1}
Coal rate kg·tHM^{-1}	500
Coke	350
PCI	150 (↓)

Table 7
Limitation of MTB/HTB/MCB/HCB co-firing in PCI system based on combustibility.

Sample	Maximum injection limit with combustibility (wt%)
MTB	< 3
HTB	> 5
MCB	> 5
HCB	< 3

acceptable range when the blending ratio surpassed approximately 27%–30%, requiring adjustment of the total fuel injection rate to maintain the heat input. In addition, due to its high ash content, HCB must be blended in a low ratio to ensure operational stability.

The economic feasibility of biocarbon injection is increasingly influenced by the global expansion of emission trading systems (ETS) aimed at achieving carbon neutrality. According to Intergovernmental Panel on Climate Change (IPCC) guidelines and most national ETS accounting frameworks, CO_2 produced from biogenic carbon is considered carbon-neutral and is therefore excluded from net emission calculations. Consequently, replacing a portion of fossil-based PCI coal with biocarbon results in a proportional reduction in net CO_2 emissions. Assuming that full oxidation of 1 t of carbon generates approximately 3.67 t of CO_2, substituting 10% of PCI carbon with biocarbon corresponds to an estimated reduction of ~0.09 t CO_2 per ton of PCI fuel.

Applying recent European Union (EU) ETS carbon credit prices (≈ 78 EUR·(t CO_2)$^{-1}$, ≈ 85 USD·t^{-1}) [49], this emission reduction translates to an economic benefit of approximately 7 USD per ton of PCI. Beyond direct fuel substitution, this credit-based cost reduction contributes to lowering overall carbon compliance costs and strengthens the economic viability of sustainable BF operation. Therefore, biocarbon injection provides not only a practical pathway for immediate CO_2 mitigation, but also a quantifiable economic advantage under carbon trading markets, reinforcing its role as a feasible transition strategy for low-carbon ironmaking.

4. Conclusions

This study assessed the applicability of biocarbons in the PCI system of the BF process and investigated their combustion behaviors and flame characteristics under co-firing conditions. Furthermore, based on the experimental results, the maximum feasible injection limits of biocarbon materials, such as torrefied biochar, which are currently gaining attention, were analyzed. The evaluation was conducted using TGA, DTF, and LFR experiments to characterize combustion and flame behavior, and the injection limits were determined by assessing the influence of the HHV and ash content. The major results can be summarized as follows.

As torrefied biomass underwent further carbonization into biocarbon, the E_a values gradually approached those of PCI coal. This indicates that the combustion behavior of biocarbons is increasingly similar to that of conventional PCI coal.

Co-firing tests showed that low blending ratios (3%) of the biocarbon samples slightly reduced combustibility, but higher ratios improved performance, especially with thermally treated samples such as HCB. Radiocarbon analysis confirmed that most of the UBC originated from PCI coal, with minimal contribution from biocarbons. For HTB and MCB, combustion improvement was mainly due to biocarbon fragmentation, leading to reduced UBC from a 3% blending ratio. HCB, owing to its moderate volatile content and active fragmentation, consistently exhibited enhanced combustion as the blending ratio increased, indicating its strong potential for PCI co-firing applications.

A fixed coke rate and varying biocarbon injection ratios were assessed based on combustion behavior, heating value (±5% of PCI coal), and ash content (<10%). MTB and HCB exceeded the heating value threshold at approximately 27%–30% blending, indicating the need to reduce total injection to maintain thermal balance. HCB also required a lower blending ratio because of its high ash content, which may affect its operational stability.

These findings show the strong potential of biomass as a PCI substitute, offering a feasible low-carbon pathway for existing BF systems.

In addition, the co-firing combustion behavior observed in this study is consistent with previously reported LFR-based raceway visualization research. Lee et al. [45] demonstrated that fuels with higher volatile content exhibited pronounced volatile-cloud flame regions and shorter char combustion lengths, whereas highly carbonized fuels tended to show extended burnout zones with limited flame luminosity, particularly under oxygen-enriched conditions. These trends agree with the present observation that MTB and HTB promote early volatile-driven ignition, while biocarbon

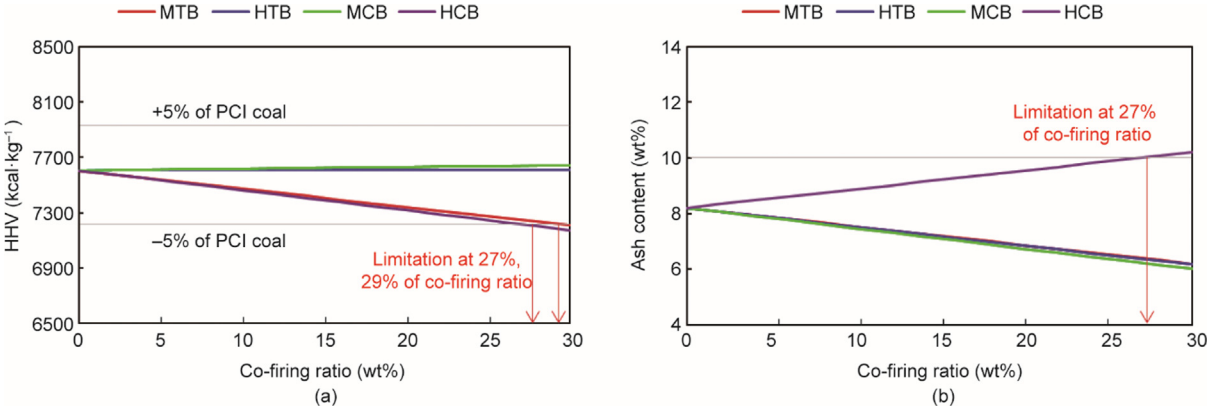

Fig. 10. Limitation of BCs co-firing in PCI system based on (a) HHV and (b) ash contents.

samples subjected to higher carbonization severity (e.g., HCB) exhibit improved char oxidation owing to increased internal pore accessibility and combustion stability at elevated blending ratios. Furthermore, the progressive reduction in UBC with increasing blending ratio for HCB aligns with the enhanced burnout efficiency reported for alternative solid fuels showing fragmentation-assisted exposure of fresh reactive surfaces during char combustion. Taken together, the findings of this study reinforce and expand upon existing literature by clarifying how the degree of biomass carbonization influences co-firing dynamics in PCI conditions.

However, the influence of alkali and trace metallic species (e.g., K, Na, and Zn) present in biocarbon ash on coke reactivity, slag behavior, and hot-metal quality should be considered in practical PCI applications. Although these effects were not addressed in the present study, which focused on combustion characteristics, previous work suggests that alkali recycling and mineral-induced phase changes may play non-negligible roles during long-term furnace operation. Therefore, further research involving ash fusion behavior, slag–metal interaction, and alkali circulation dynamics will be required to evaluate the metallurgical compatibility of biocarbon at industrial injection levels.

Although hydrogen-based direct reduction is widely regarded as a long-term solution for achieving near-zero carbon ironmaking, its industrial implementation is currently limited by renewable hydrogen supply, infrastructure availability, and the need for major process transitions. In contrast, most operating BFs are expected to remain in service over the next several decades, particularly in regions where large-scale capital replacement is difficult. In this context, biocarbon injection into existing PCI systems can function as a bridge technology, providing immediate and incremental CO_2 reduction without requiring substantial modifications to furnace operation. Therefore, the present findings highlight the role of biocarbon co-firing as a practical transitional pathway that complements, rather than replaces, future hydrogen-based ironmaking strategies.

CRediT authorship contribution statement

Min-Woo Kim: Writing – review & editing, Writing – original draft, Visualization, Validation, Methodology, Investigation, Formal analysis, Conceptualization. **Min-Jong Ku:** Methodology, Investigation. **Jongho Kim:** Resources, Methodology. **Gyoung-Min Kim:** Investigation, Data curation. **Chung-Hwan Jeon:** Supervision, Project administration. **Dae-Gyun Lee:** Writing – review & editing, Writing – original draft, Visualization, Validation, Methodology, Investigation, Conceptualization.

Declaration of competing interest

The authors declare that they have no known competing financial interests or personal relationships that could have appeared to influence the work reported in this paper.

Acknowledgments

This research was supported by grants from the National Research Foundation of Korea, funded by the Ministry of Science, ICT, and Future Planning (2022K1A4A8A01080312) and by the Regional Innovation System & Education (RISE) program through the institute for Regional Innovation System & Education in Busan Metropolitan City, funded by the Ministry of Education (MOE) and the Busan Metropolitan City, Republic of Korea (2025-RISE-02-004-11970001-01).

Appendix A. Supplementary data

Supplementary data to this article can be found online at https://doi.org/10.1016/j.eng.2025.12.004.

References

[1] Emissions measurement and data collection for a net zero steel industry. Report. Paris: International Energy Agency; 2023.
[2] Wang C, Nilsson L, Larsson M, Boden A, Sundqvist L, Wikstrom J. Alternative fuels injection to BF and their impacts to the integrated steel works. In: Proceedings of International Conference on Process Development in Iron and Steelmaking; 2012. TIB; 2012. p. 557–66.
[3] Blast furnace CO_2 reduction initiatives. Report. Tokyo: JFE Steel Corporation; 2013.
[4] Fan Z, Friedmann SJ. low-carbon production of iron and steel: technology options, economic assessment, and policy. Joule 2021;5(4):829–62.
[5] Yi SH, Choi ME, Kim DH, Ko CK, Park WI, Kim SY. FINEX® as an environmentally sustainable ironmaking process. Ironmak Steelmak 2019;46:625–31.
[6] Exploring hydrogen with POSCO #3: the future of steel—Hydrogen-based steelmaking. Report. Pohang: POSCO Newsroom; 2021.
[7] The future of hydrogen. Report. Paris: International Energy Agency; 2019.
[8] Ishaq H, Dincer I, Crawford C. A review on hydrogen production and utilization: challenges and opportunities. Int J Hydrogen Energy 2022;47:26238–64.
[9] Sun M, Pang K, Barati M, Meng X. Hydrogen-based reduction technologies in low-carbon sustainable ironmaking and steelmaking: a review. Renew Sustain Energy Rev 2024;10:10–25.
[10] Lee DG, Kim MW, Bae YH, Kim KM, Kim GM, Jeon CH. FINEX PCI fuel diversification for techno-economical operations: impact of high-volatile coal agglomeration on combustion. Fuel 2025;381:133582.
[11] Japan's Kobelco to use torrefied biomass in steelmaking. Report. London: Argus Media group; 2025.
[12] Decarbonizing steel: how biochar is reshaping the industry. Report. Raipur: BigMint; 2024.
[13] Q&A: US cleantech firm to start biochar plant in Quebec. Report. London: Argus Media group; 2025.
[14] Minnesota biochar and the future of making steel. Report. Duluth: Natural Resources Research Institute; 2024.
[15] Wang S, Chai Y, Wang Y, Luo G, An S. Review on the application and development of biochar in ironmaking production. Metals 2023;13:1844.
[16] Ibitoye SE, Loha C, Mahamood RM, Jen TC, Alam M, Sarkar I. An overview of biochar production techniques and application in iron and steel industries. Bioresour Bioprocess 2024;11:65.
[17] Suopajärvi H, Umeki K, Mousa E, Hedayati A, Romar H, Kemppainen A. Use of biomass in integrated steelmaking—status quo, future needs and comparison to other low-CO_2 steel production technologies. Appl Energy 2018;213:384–407.
[18] Li B, Li D, Hu J, Zhu X, Wang H, Jeon CH, et al. Carbon emission of municipal solid waste under different classification methods in the context of carbon neutrality: a case study of Yunnan Province, China. Fuel 2024;372:132167.
[19] Quan S, Zeng Y, Wu Y, Kim R-G, Li Z, Han Y, et al. Ash thermomechanical properties and combustion characteristics during co-combustion of anthracite and biomass for CFB combustors. Biomass Bioenergy 2025;198:107868.
[20] Yang X, Li D, Zhu X, Zhu T, Mun TY, Wang H, et al. Interaction of ilmenite oxygen carrier with wheat straw ash during chemical looping combustion: mechanisms and performance variation. Fuel 2024;374:132434.
[21] Wang X, Yang X, Yang H, Zhang M, Zhou T, Zhu X, et al. Fate of phosphate compounds during chemical looping combustion of agrofuel: impacts on physical–chemical properties of ilmenite and mechanisms. Powder Technol 2025;461:121097.
[22] Quan S, Mei J, Li D, Huang Y, Li Z, Zhu X, et al. A comprehensive evaluation of kinetic reaction mechanisms for NO and N_2O emissions during NH_3/H_2 combustion across multi-temperature regimes. J Energy Inst 2025;123:102260.
[23] Zhang A, Li D, Zhu X, Kim GM, Zeng Y, Jeon Ch, et al. A molten salt-mediated biomass gasification process for high-yield hydrogen production with *in situ* carbon capture: experiments, simulation and ANN prediction. Energy Convers Manag 2025;332:119735.
[24] Lee BH, Sh L, Lee DG, Jeon CH. Effect of torrefaction and ashless process on combustion and NO_x emission behaviors of woody and herbaceous biomass. Energies 2021;151:106133.
[25] Noh YH, Lee DG, Park JH, Song GS, Kim JS, Park SJ, et al. Ashless herbaceous biomass for slagging and fouling reduction in solid-fuel boiler. Fuel 2025;379:132957.
[26] Jannisa K, Attaso K, Wipawee D. Waste-to-energy conversion of rubberwood residues for enhanced biomass fuels: process optimization and eco-efficiency evaluation. Energies 2024;17(21):5444.
[27] Bhautik G, Uplabdhi T, Anil KS, Mithilesh KJ. Impact of torrefaction on thermal behavior of wheat straw and groundnut stalk biomass: kinetic and thermodynamic study. Fuel Commun 2022;112:100073.
[28] Lee DG, Lee JH, Kim GM, Jeong JS, Kim SM, Jeon CH. The initial ash deposition formation in horizontal combustion reactor for blending torrefied biomass wood pellet and coals. Renew Energy 2024;226:120198.
[29] Kim GM, Choi JH, Jeon CH, Lim DH. Effects of cofiring coal and biomass fuel on the pulverized coal injection combustion zone in blast furnaces. Energies 2022;15:655.
[30] Evaluation of combustion behaviour of coal blends for PCI. Report. Brisbane: ACARP; 2020.
[31] Du SW, Chen WH, Lucas JA. Pulverized coal burnout in blast furnace simulated by a drop tube furnace. Energy 2010;35(2):5576–81.

[32] Stančin H, Mikulčić H, Manić N, Stojiljiković D, Vujanović M, Wang X, et al. Thermogravimetric and kinetic analysis of biomass and polyurethane foam mixtures co-pyrolysis. Energy 2021;237:121592.
[33] Zhai M, Guo L, Zhang Y, Dong P, Qi G, Huang Y. Kinetic parameters of biomass pyrolysis by TGA. BioResources 2021;16:7428–43.
[34] Standard test method for moisture in the analysis sample of coal and coke. Report. West Conshohocken: Advancing Standards Transforming Markets International; 2025.
[35] Standard test method for volatile matter in the analysis sample of coal and coke. Report. West Conshohocken: Advancing Standards Transforming Markets International; 2025.
[36] Standard practice for proximate analysis of coal and coke. Report. West Conshohocken: Advancing Standards Transforming Markets International; 2021.
[37] Standard test method for ash in the analysis sample of coal and coke from coal. Report. West Conshohocken: Advancing Standards Transforming Markets International; 2020.
[38] Standard test methods for determination of carbon, hydrogen, and nitrogen in analysis samples of coal and coke. Report. West Conshohocken: Advancing Standards Transforming Markets International; 2021.
[39] Standard test method for gross calorific value of coal and coke. Report. West Conshohocken: Advancing Standards Transforming Markets International; 2019.
[40] Anthony DB, Howard JB. Coal devolatilization and hydrogasification. AIChE J 1976;22:625–56.
[41] Li H, Elliott L, Rogers H, Wall T. Comparative study on the combustion performance of coals on a pilot-scale test rig simulating blast furnace pulverized coal injection and a lab-scale drop-tube furnace. Energy fuels 2025;28:363–8.
[42] Stuiver M, Polach HA. Discussion reporting of ^{14}C data. Radiocarbon 1977;19:355–63.
[43] Klein MG, Mous DJW, Gottdang A. A compact 1MV multi-element AMS system. Nucl Instrum Methods Phys Res Sect B 2006;249:764–7.
[44] Bae YH, Lee DG, Kim KM, Kim MW, Zeng Y, Jeon CH. Numerical analysis of fuel-flexible FINEX PCI raceway: natural gas co-firing with advanced coal fragmentation model. Energy 2025;319:135061.
[45] Lee DG, Kim MW, Ku MJ, Bae YH, Kim KM, Kim GM. Combustion visualization analysis of alternative fuels in the pulverized coal injection raceway through laminar flow reactor. Heliyon 2024;10:e36238.
[46] Bennett P, Fukushima T. Impact of PCI coal quality on blast furnace operations. Report. Brisbane: ACARP; 2007.
[47] Queensland high energy coals for the PCI market—advantages for low volatile coal. Report. Queensland: Queensland Government.
[48] Carpentar AM. Use of PCI in blast furnaces. Report. Paris: IEA Clean Coal Centre; 2006.
[49] Sitarz J, Pahle M, Osorio S, Luderer G, Pietzcker R. EU carbon prices signal high policy credibility and farsighted actors. Nat Energy 2024;9:691–702.